Oxidation pathways towards Si amorphous layers or nanocrystalline powders as Li-ion batteries anodes

Kamal Annou, Mathilde Pelosi, Gregory Gershinsky, Frédéric Favier, Yvan Cuminal, Monique Tillard, David Zitoun

Mater Renew Sustain Energy (2014) 3:32
DOI 10.1007/s40243-014-0032-7

ORIGINAL PAPER

Oxidation pathways towards Si amorphous layers or nanocrystalline powders as Li-ion batteries anodes

Kamal Annou · Mathilde Pelosi · Gregory Gershinsky · Frederic Favier · Yvan Cuminal · Monique Tillard · David Zitoun

Received: 15 January 2014 / Accepted: 1 May 2014 / Published online: 30 May 2014

Abstract Silicon nanomaterials are obtained by an original approach based on the direct solution phase oxidation of a solid state Zintl phase NaSi used as silicon precursor. Alcohols with different alkyl chains are chosen as oxidizing agents. The materials are characterized by X-ray diffraction, scanning electron microscopy, transmission electron microscopy and Raman spectroscopy. The most relevant parameter lies in the amorphous character of the silicon nanoparticles produced by this route. Amorphous nature of silicon is one of the key features for succeeding in the improvement of anodes for Li-ion batteries. The Si nanostructures have been tested as anodic materials for lithium ion batteries.

Keywords Silicon · Amorphous · Nanoparticles · Nanomaterial · Layers · Li-ion · Battery

K. Annou · M. Pelosi · F. Favier · M. Tillard
Institut Charles Gerhardt, UMR 5253, Université de Montpellier II, Sciences et Techniques du Languedoc, CC015, 2 Place Eugène Bataillon, 34095 Montpellier Cedex 5, France
e-mail: mtillard@univ-montp2.fr

K. Annou · Y. Cuminal
Institut d'Electronique du Sud, UMR5214, Université de Montpellier II, Sciences et Techniques du Languedoc, 2 Place Eugène Bataillon, 34095 Montpellier Cedex 5, France

G. Gershinsky · D. Zitoun (✉)
Department of Chemistry, Bar Ilan Institute of Nanotechnology and Advanced Materials, Bar-Ilan University, 52900 Ramat Gan, Israel
e-mail: david.zitoun@biu.ac.il

Introduction

The success in colloidal bottom-up approach synthesis of Si has been more limited than the textbook examples of ionic semiconductors after some early successes and synthesis pathways investigation still worthwhile [1].

Early examples of gas phase syntheses have been reported for the preparation of well-defined silicon nanocrystals [2] and nanowires [3]. The common precursors used in chemical vapor deposition (CVD) are silanes (like SiH_4 or Si_2H_6) or chlorosilanes, which undergo thermal decomposition or hydrogenolysis, in presence of a metal catalyst. Vapor–liquid–solid mechanism leads to the formation of smooth single crystalline Si nanowires [4, 5]. These routes have been adapted to the synthesis in high boiling point solvents from a very expensive Si_3H_8 precursor to yield amorphous Si particles [6] or crystalline nanowires using a solution–liquid–solid (SLS) mechanism [7]. A successful alternative route to size-controlled Si nanoparticles consists in the thermal decomposition of hydrogen silsesquioxane at high temperature [8].

Examples of solution routes are sparser and involve the reduction of a silicon halide ($SiCl_4$, $RSiCl_3$) by a strong reducing agent [9], butyl-lithium, naphthalides [10–12] or hydrides [13, 14], in presence of a surfactant to limit the nanoparticles growth and coalescence but the surfactant shell impedes their use for electrochemical applications. Alternatively, Si nanowires are electrochemically deposited by step-edge decoration of highly oriented pyrolytic graphite (HOPG) from a platting solution of $SiCl_4$ in aprotic ionic liquid [15].

Therefore, the use of silicon Zintl phases, characterized by the coexistence of Si polyatomic anionic clusters and alkaline or alkaline earth cations, stands as a valuable and simple route towards Si nanostructures. The Kauzlarich

group has first developed this pathway by varying the Zintl phase (NaSi or Mg_2Si) dispersed in a solvent, the oxidative agent (such as $SiCl_4$) and the capping agent (Grignard reagent or alkyl lithium) [16–20]. This pioneering work has been followed by in-depth analysis of the quantum size effect on size-selected nanocrystals [21]. Solid state oxidation of Zintl phase also yields embedded Si nanocrystals [22]. Soft oxidation of germanium Zintl phases by alcohols yields crystalline nanoparticles of Ge with potential applications in batteries [23].

The appealing ability to perform a room temperature synthesis of amorphous silicon and the need for better understanding of the reaction pathways, drive us to study the reactivity of silicon anionic clusters (Zintl phases) under oxidation with mild reducing agents.

In this manuscript, we report on the preparation of Si nanoparticles by direct oxidation of Si Zintl anions by anhydrous alcohols. The NaSi Zintl phase serves as Si precursor. Crystallinity, particle size and reaction completion are investigated as a function of the chain-length of the alcohol. The crystallinity has been carefully studied by Raman spectroscopy. The preliminary electrochemical tests as anodic material emphasize the potential application in Li-ion batteries.

Experimental section

Sodium (lingot Na from Merck-Schuchardt, >99 %) is scraped to remove surface impurities and then stored in a glove box filled with dry Ar. Silicon (Si, −325 mesh, 99 %) is purchased from Sigma-Aldrich. Anhydrous alcohols are stored and handled in the glove box: ethanol (Acros Organics, >99 %) 1-butanol (Sigma-Aldrich, >99 %), benzyl alcohol (Acros Organics, 99 %), 1-octanol (Sigma-Aldrich, >99 %).

The NaSi Zintl phase is prepared from stoichiometric proportions of the elements mixed in a weld-sealed stainless steel tube. The Na/Si mixture is heated to 920 K for 2 days during which the reactor is shaken several times to improve homogenization of the melt and then cooled to room temperature at the rate of 40°/h. The air-sensitive products of reactions are handled in the glove box.

Nanoparticles are obtained by direct oxidation of the solid precursor by an alcohol. The NaSi powder (100 mg) is slowly added to 10 mL of anhydrous degassed alcohol under stirring in a glove box or in a Schlenk connected to a vacuum line. The reaction time is optimized for completion of the reaction, and the solution is left to stir for 15–60 min, a time beyond which no major change in the product is observed. At the end of the reaction, the black powder (Si nanoparticles) is separated by centrifugation and washed with anhydrous ethanol. The yield of the reaction is more than 90 %, the only loss coming from the washing steps.

Transmission electron microscopy (TEM) is performed with a JEOL 1200 EX II microscope operating at 100 kV accelerating voltage. The X-ray diffraction patterns are recorded on a Philips analytical X'pert diffractometer equipped with a copper tube and a hybrid monochromator (parabolic multilayer mirror and two-crystal, Cu Kα radiation). The Raman spectroscopy is carried out using a LAbRam Aramis IR^2 spectrometer equipped with a helium neon laser (633 nm). The power of the laser beam is estimated to a maximal value of 6 mW at the sample surface. The use of various filters (named D0.6, D1 and D2) allows a reduction of intensity to 200, 70 and 50 μW, respectively. Scanning electron microscopy (SEM) images are collected on a FEI Magellan equipped with an energy-dispersive X-ray (Oxford 80 mm^2) spectroscopy (EDS) attachment. EDS has been typically collected on images of 25 μm^2 to provide a reliable composition.

Anodes are tested in coin-type cells (2523, NRC, Canada) versus lithium metal (Chemetall Foote Corporation, USA). Electrolyte solution is fluoro-ethylene carbonate (FEC) (Aldrich, <20 ppm water) and dimethyl carbonate (DMC) (Aldrich, <20 ppm water) (1:4 ratio) with 1 M $LiPF_6$ (Aldrich). The cells are assembled in an argon-filled glove box, with a purifying system (MBraun GmbH, Germany), oxygen and water contents below 1 ppm.

Cyclic voltammetry is measured at 30 °C with a Bio-Logic VMP3, multi-channel potentiostat at 1 mV/s between 0.8 and 0.0 V versus Li^+/Li which accounts for a charge and discharge duration of 800 s. The charge capacities, discharge capacities and coulombic efficiencies are calculated in the EC Lab software from the same data.

Results and discussion

Precursor characterization

Si nanoparticles have been prepared from the oxidation of a Zintl phase used as Si precursor (Fig. 1). The NaSi Zintl phase is prepared from the elements by high temperature synthesis. The Rietveld refinement (program Jana) of its experimental XRD powder pattern leads to good agreement factors of $R_p = 2.04$, $R_{wp} = 2.85$ and $\chi^2 = 2.59$ (Fig. 1b). Parameters of the unit cell C2/c; $a = 12.1816$ (5) Å; $b = 6.5541$ (3) Å; $c = 11.1690$ (4) Å and $\beta = 119.010$ (2), values that agree well with those previously reported [24, 25]. The structure of NaSi is built on discrete anionic units, Si_4^{4-}, packed together with sodium cations (Fig. 1a). The NaSi Zintl compound can be formally described as $[Na^+]_4[Si_4^{4-}]$.

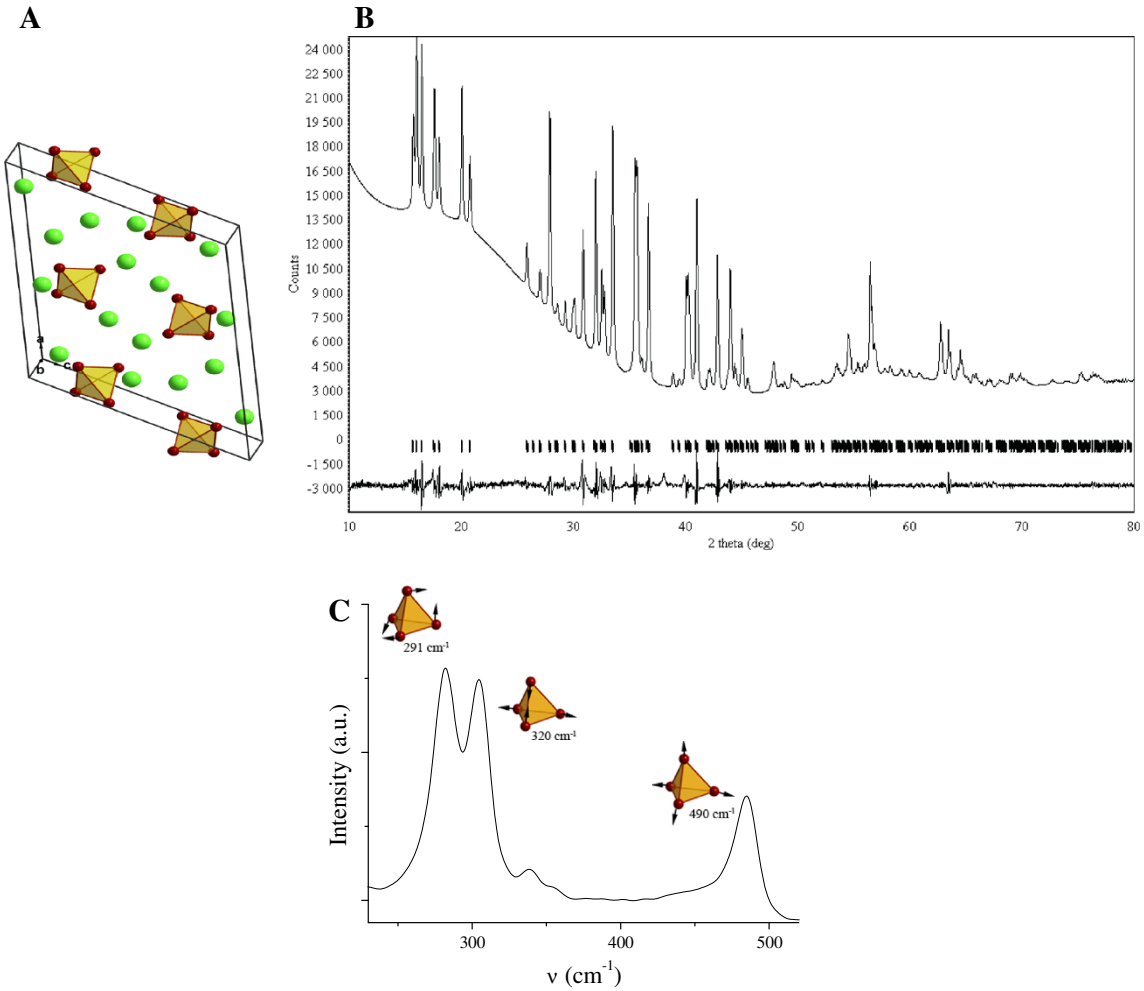

Fig. 1 Representation of the NaSi structure (viewed along *b*-axis) emphasizing the Si_4^{4-} anionic clusters (**a**); X-ray powder diffraction pattern of NaSi, corresponding Bragg positions and Rietveld refinements results (**b**); Raman spectrum of NaSi in the 225–525 cm^{-1} wave number range with the corresponding vibration modes of the Si_4^{4-} clusters (**c**)

Raman spectroscopy is a complementary technique for the full identification of NaSi. The Si_4^{4-} unit (symmetry Td) is characterized by three Raman active vibration modes $A_1(\nu_1)$, $T_2(\nu_3)$ and $E(\nu_2)$, respectively observed at 490, 320 and 291 cm^{-1} (Fig. 1c), consistent with previously reported Raman spectrum [26]. Raman spectroscopy confirms the presence of Si_4^{4-}, in addition to XRD results, and allows the complete and unambiguous identification of the compound NaSi.

Oxidation process

Alcohols are chosen as oxidizing agents for their mild reducing character and their availability. Furthermore, alcohols traces can be easily removed from the surface after synthesis [23]. The alcoholic proton reacts with the Zintl phase to give gaseous H_2 and alkoxide (which protonates upon exposure to air). Indeed, the reaction occurs with gas release and no other by-product has been noticed from ^{1}H-NMR spectrum of the supernatants.

The reaction is carried out using powdered NaSi with anhydrous alcohol as oxidizing agent. Various alcohols are tested including ethanol, 1-butanol, benzyl alcohol and 1-octanol. Powder XRD analyses of products show that NaSi reacts completely during the oxidation reaction (Fig. 2a). In all cases, products of reaction are nanosized and quite amorphous as proved by the wide peaks centered around 29° and 55° angular positions. Sometimes small and narrow peaks are observed that could be indexed within the cubic diamond-type structure of silicon. This crystalline phase is rather an impurity than a product of the reaction and most of the sample can be considered as nanocrystalline or amorphous. Therefore, Raman spectroscopy brings much more information on the nature of the products.

Actually, Raman lines are actually characterized by their shape (width, symmetry) and their position,

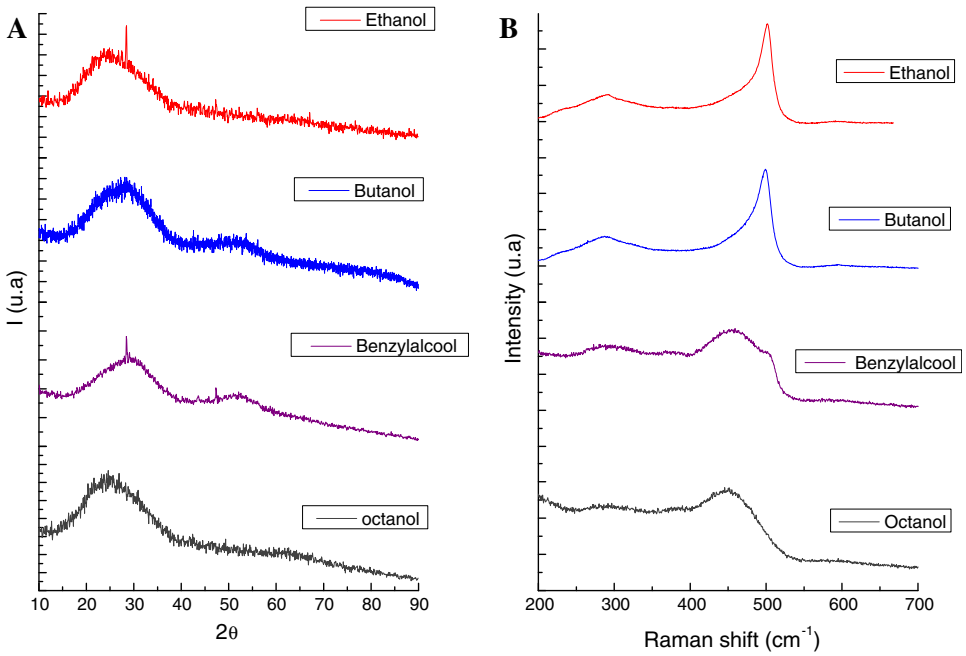

Fig. 2 XRD of Si nanopowders for each oxidizing solvent (**a**); Raman spectra of Si nanopowders for each oxidizing solvent (**b**)

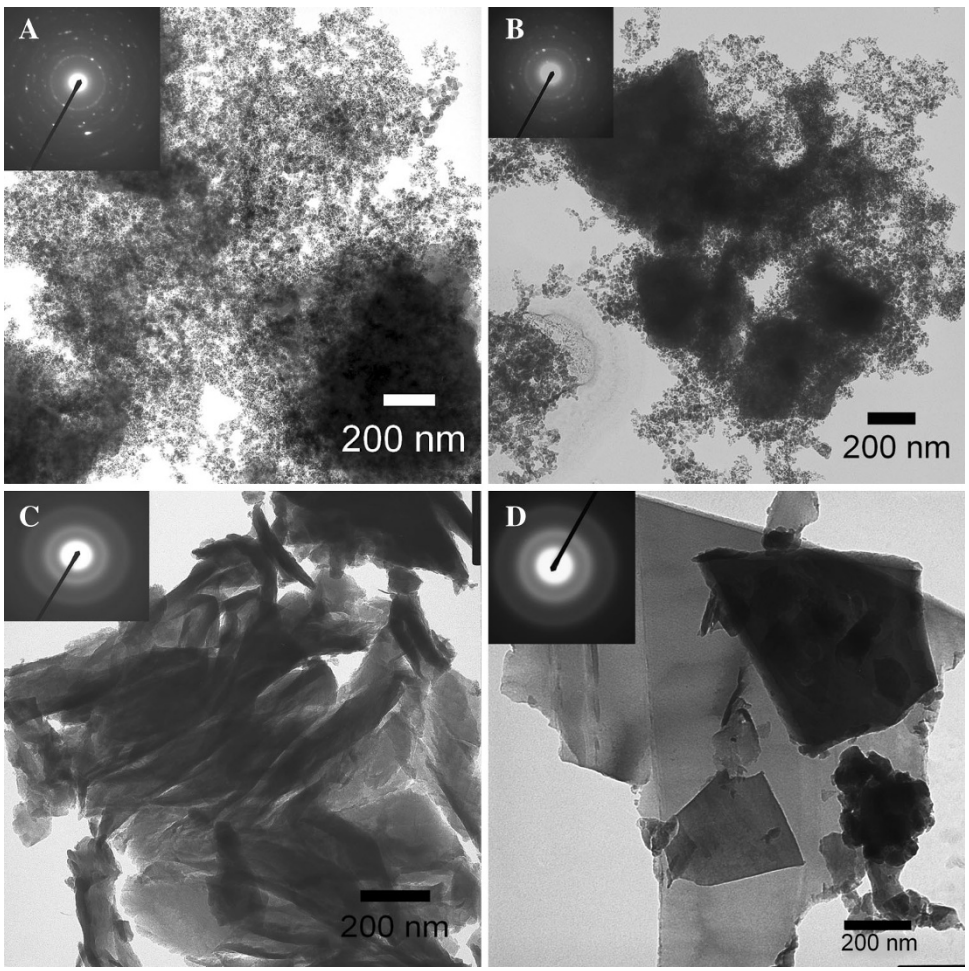

Fig. 3 TEM micrographs of Si nanoparticles from ethanol (**a**); 1-butanol (**b**); benzyl alcohol (**c**); 1-octanol (**d**) (*insets*: SAED)

parameters that are strongly correlated with the structure/morphology (crystalline, amorphous) and with the particle size (micrometric, nanometric). The Raman band position is dependent on the particle size, shifted towards low wave numbers when the average particle size decreases, and broadened when the amorphous character increases [27].

Their spectra, shown in Fig. 2b, present a large and asymmetric band clearly shifted from the position of the Raman line attributed to crystalline silicon (Si–Si stretch at 521 cm^{-1}). The experimental Raman spectrum is fitted using two Gaussian functions centered at 501 and 460 cm^{-1}. The contribution at 501 cm^{-1} is assigned to the nanocrystalline part while that at 460 cm^{-1} corresponds to the amorphous part of the sample (surface and/or amorphous NPs) [28, 29]. The products can be classified into two groups: short chain alcohols (ethanol and 1-butanol) yield mainly nanocrystalline Si with a band at 501 cm^{-1}, while benzyl alcohol and 1-octanol yield mainly amorphous Si with a main band at 460 cm^{-1}. The trend in crystallinity is consistent with a previous investigation of Ge Zintl phase oxidation process [23].

Electron microscopy provides an excellent tool for measuring crystallinity, morphology and elemental composition. For each of the synthesis, the product can be easily dispersed in ethanol without any surfactant or ligand. Selected area electron diffraction (SAED) of the products show two typical patterns. In the case of short chain alcohols (Fig. 3a, b, insets), the nanoparticles display a diffraction pattern where rings could be indexed into the cubic diamond-type structure of Si. On the other hand, for benzyl alcohol and 1-octanol, the electron diffraction is very diffuse and relates to amorphous Si.

Concerning the morphology, using a short linear alcohol (ethanol and 1-butanol), TEM shows chains of particles where the particle size depends on the nature of the oxidizing agent. Nanoparticles of 15 ± 4 nm in diameter are obtained from ethanol while particles of 11 ± 4 nm in diameter, with a larger size distribution, are obtained from 1-butanol. In the case of aromatic backbone (benzyl alcohol), TEM shows large submicronic sheets of amorphous materials without any individual particles or networks. The sheets are very thin (<20 nm) since TEM reveals several sheets oriented perpendicular to the grid. Using 1-octanol, the sheets are even larger, beyond micron in size, while the thickness remains nanometric. A reliable measurement of the thickness could not be obtained on this sample since all the sheets are laying on the TEM grid. The control of morphology obtained by varying the solvents can be understood from the difference of reactivity of alcohols towards alkaline elements. It is well established that the hydrogen evolution upon exposure of alkali metals (or Zintl phase) to alcohols depends on the chain length. Reacting with a long chain alcohol is therefore recommended to avoid uncontrollable reactions.

Ethanol and 1-butanol react faster than benzyl alcohol and 1-octanol, yielding nanocrystalline particles. The exothermic character of the reaction causes a local elevation of temperature, a factor that could favor the crystallization of Si.

On the other hand, benzyl alcohol and 1-octanol react slowly towards the Zintl phase and yield an amorphous material with a sheet morphology and dimensions that could be compared with the initial size of the NaSi grains. The soft solvolysis retains the size of the grains but yields a 2D morphology which can be accurately observed on scanning electron micrographs. On Fig. 4, we display the SEM of the different products. The powders present a layered structure on the micron scale for all the products. The platelets are even present in the case of short chain alcohols, for which TEM displays chains of particles. Obviously, the particles are aggregated into a layered material. In the case of benzyl alcohol and 1-octanol, SEM confirms the layered structure of the material with nanoscale thickness and micron scale length.

The formation pathway of the layered materials may arise from the formation of alcohol layers on the surface of the Zintl phase during reaction. Benzyl and octyl moieties are well known to pack as self-assembled monolayers. In particular benzyl alcohol results in layered materials in the case of non-aqueous sol–gel synthesis [30]. Octyl moieties are also long enough to form self-assembled monolayers, which could explain the larger sheets obtained in that case. Moreover, Zintl phase also forms layered compounds and a layered intermediate Na_xSi ($x < 1$) could induce the formation of layered amorphous silicon. To strengthen this assumption, we have measured the Na content in all the samples.

The purity of the material is investigated by energy-dispersive X-ray spectroscopy (EDS) (Fig. 5). All the samples show a high atomic content of Si (above 70 %) with oxygen and sodium as main other elements. The presence of Na is expected since the Zintl phases are also known to result in the formation of clathrates with a significant amount of residual alkaline element [31]. Na amount depends on the alcohol used during the synthesis with a very large discrepancy between the two main groups of oxidizing alcohols. The presence of significant Na content (6.8 % for 1-octanol and 8.0 % for benzyl alcohol) is consistent with the amorphous nature of Si observed for the corresponding samples. Such a high level of impurities can only be accommodated by a high density of defects, i.e. amorphous Si. On the contrary, short chain alcohols yield very low Na content (ethanol 2.4 %, 1-butanol 1.6 %), consistent with the

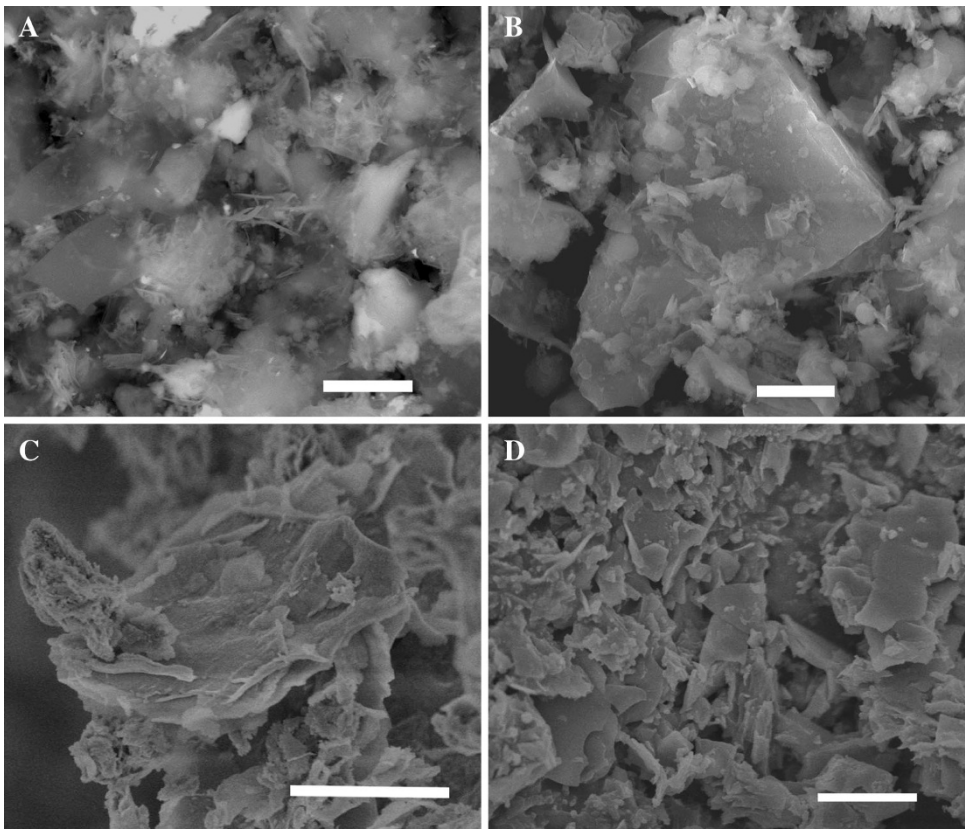

Fig. 4 SEM micrographs of Si nanoparticles from ethanol (**a**); 1-butanol (**b**); benzyl alcohol (**c**); 1-octanol (**d**). (*Scale bar* 2 μm)

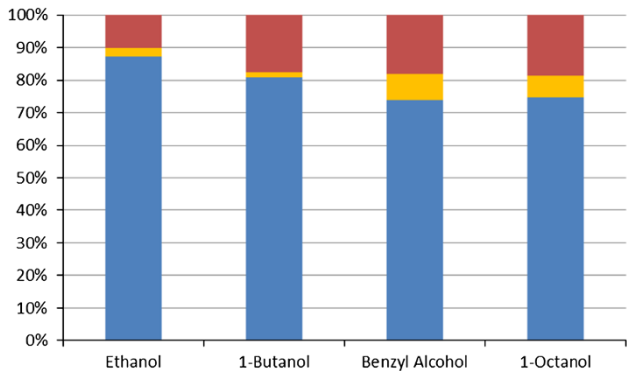

Fig. 5 Elemental atomic composition from EDS on the different samples (Si: *Blue*, Na: *Yellow*, O: *Red*)

nanocrystalline structure where Na is trapped at the developed defective surface. Interestingly, the oxygen content, which can also come from the environment and during post-synthesis storage in air, stays low: 10.2 % only even after exposure to air for several weeks.

The high Si atomic ratio, together with the amorphous or nanocrystalline structure of these materials, makes these products of high interest as anodic materials for Li-ion batteries. The presence of Na impurities is a priori not detrimental since they would be easily replaced by Li during the electrochemical process.

Electrochemical experiments

Si has an outstanding theoretical specific capacity while used as anode material in Li-ion batteries (3,600 vs. 372 $mA.g^{-1}$ for carbonaceous commercial anodes) but bulk Si does not cycle [32]. To address this issue, several routes have been explored which include the use of amorphous [33] or nanostructured [34] silicon thin films, silicon nanowires [5] and, very generally in a broader approach, any nanostructured silicon material [35]. Nanocrystalline silicon has shown remarkable coulombic efficiency when deposited as a thin film on Cu [36]. Nevertheless, the elaboration pathways mentioned above are limited to very low loading of active material [37] and silicon nanopowder has attracted more attention as a readily available material to grow thicker electrodes [38]. One of the most successful routes relies on carboxy methylcellulose (CMC) binder slurry with silicon nanoparticles and carbon black [39–42]. The coulombic efficiency is maintained for hundreds of cycles for a high CMC ratio but inevitably fades [43].

In this work, we have chosen to test a low loading of active material ($\sim$0.1 mg/cm^2) without a specific formulation to test their potential applications as anodic materials. The Si powders prepared in the present work are tested against a pure lithium electrode in coin cells. In the

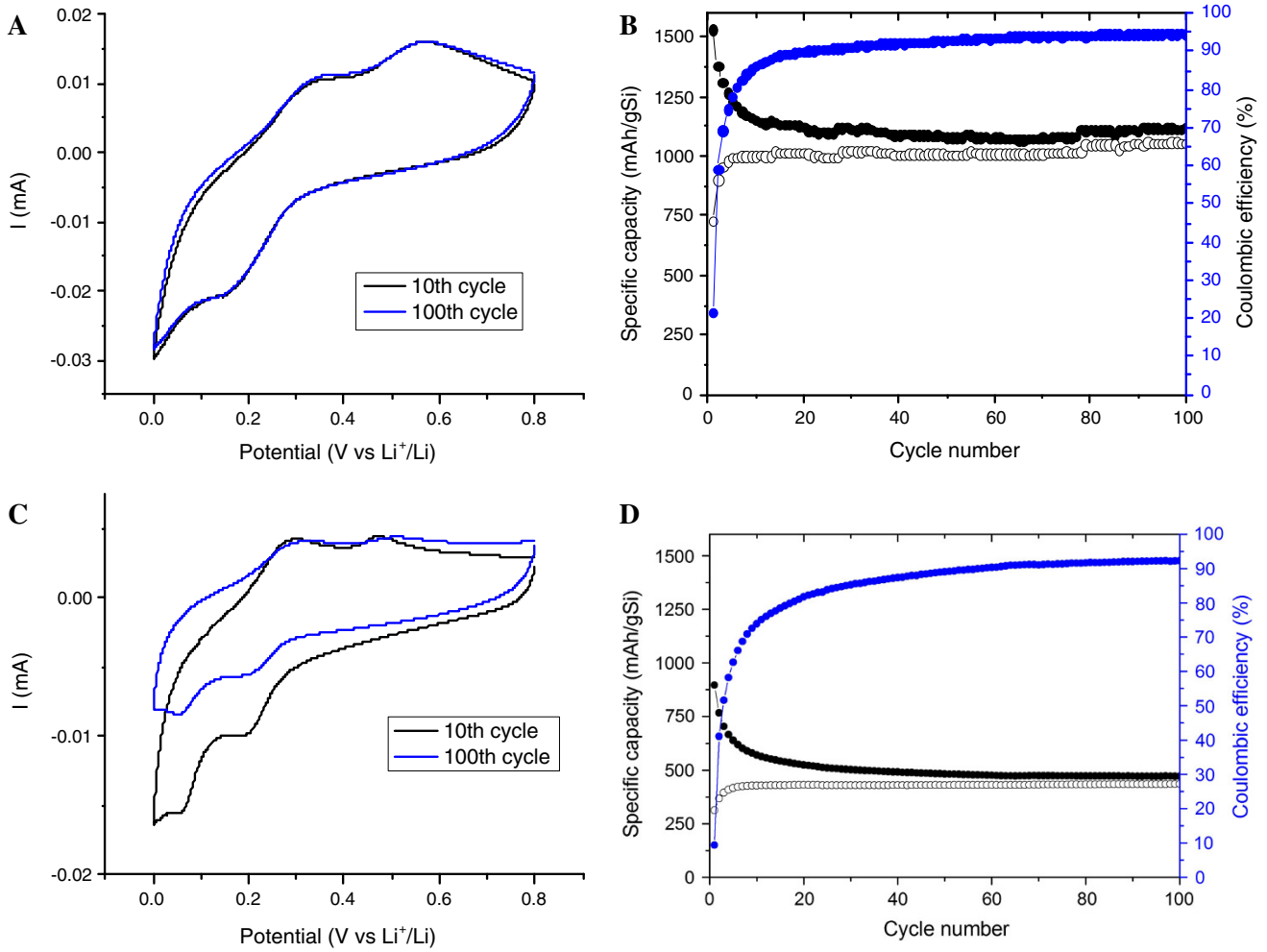

Fig. 6 Electrochemical tests at 3C on amorphous Si (from octanol synthesis: **a**, **b**) and nanocrystalline Si (from butanol synthesis **c**, **d**): cyclic voltammetry of the 10th cycle (*black line*) and 100th cycle (*blue line*) (**a**–**c**); charge capacity (*black dots*), discharge capacity (*black circles*) and coulombic efficiency (*blue dots*) (**b**–**d**)

following work on half-cell versus Li metal, we use the term: "lithiation" process to describe the discharge versus Li and "delithiation" for the charge versus Li; contrary to the full cell, where Si is the anodic material. The results are presented for two typical types of nanopowder: an amorphous sample (synthesis from octanol, Fig. 6a, b) and a nanocrystalline one (synthesis from butanol, Fig. 6c, d). For each sample, Fig. 6 presents on the left panel the cyclic voltammetry for the 10th and 100th cycles. On the right panel, Fig. 6 presents the specific charge and discharge capacities for 100 cycles (left *y* axis) together with the coulombic efficiency (right *y* axis). The main point lies in the analysis of the lithiation events and the eventual differences between the samples. For amorphous silicon, we observe two lithiation events at 0.15 and 0.02 V versus Li in discharge and delithiation at 0.36 and 0.57 V versus Li in charge (Fig. 6a). These two events correspond to the transition from Si to two main phases of Li_xSi alloys.

For nanocrystalline Si, Fig. 6c also displays two lithiation plateaus at 0.19 and 0.05 V versus Li and delithiation at 0.30 and 0.47 V versus Li slightly different from the amorphous silicon sample after 10 cycles. However, the weight of the two lithiation events in the overall capacity displays a large discrepancy, which is responsible for the large irreversibility observed for the nanocrystalline sample. On Fig. 6c, the low potential lithiation completely disappears after 100 cycles. The irreversibility of the processes results in the rapid fading of the capacity (Fig. 6d), which stabilizes at 400 mAh/g_{Si} with a coulombic efficiency of 92 % after 100 cycles.

The amorphous silicon sample displays a dominant electrochemical event at higher potential, which is extremely stable from the 10th to the 100th cycle. This reversibility results in the better capacity retention observed for amorphous silicon. The maximum lithium insertion leads to specific discharge capacity of

1,000 mAh.g^{-1} after 3 cycles and the capacity is maintained after 100 cycles. The coulombic efficiency of the amorphous Si sample reaches 95 % after 100 cycles.

The specific capacities measured in this work for amorphous and nanocrystalline Si are in the same range as initial capacities reported in the literature for other kinds of nanoscale Si. These exploratory experiments clearly prove that the electrochemical behavior is related to the crystallinity of Si. Amorphous Si has a clear edge over nanocrystalline Si.

Conclusion

Layers of Si nanomaterials can be prepared by the oxidation of a NaSi Zintl phase by an alcohol. The oxidation consists in the room temperature solvolysis of Zintl phase in anhydrous degassed alcohols. Results clearly emphasize the role of the solvent in the morphology and crystallinity of the materials. While short alcohols yield chains of nanocrystalline Si particles, aromatic and longer chains yield large flakes of amorphous Si as proven by XRD, Raman and SAED. The amorphous Si displays an interesting layered morphology and presents a high content of Na, which could be responsible for the morphology and the amorphous character. All materials display a low level of oxidation, even after storage in ambient conditions.

Preliminary results point out at the major advantage of amorphous Si versus nanocrystalline Si as anodic materials for batteries. The layered materials prepared using this original oxidation reaction are free of organic residues and, when tested in electrochemical cells, exhibit a discharge capacity of 1,100 mAh.g^{-1} after 100 cycles, twice more than the nanocrystalline samples. These results are interesting for Si anodic materials prepared by solution phase chemistry insofar and could be greatly improved by optimization of the electrode preparation.

Acknowledgments This work has been supported by the National Agency for Research (ANR Inxilicium, France) and partially supported by the Israel National Research Center for Electrochemical Propulsion—INREP (Israel Science Foundation Grant No 2797/11).

References

1. Veinot, J.G.C.: Synthesis, surface functionalization, and properties of freestanding silicon nanocrystals. Chem. Comm. **40**, 4160–4168 (2006)
2. Huisken, F., Kohn, B., Paillard, V.: Structured films of light-emitting silicon nanoparticles produced by cluster beam deposition. Appl. Phys. Lett. **74**, 3776–3778 (1999)
3. Morales, A.M., Lieber, C.M.: A laser ablation method for the synthesis of crystalline semiconductor nanowires. Science **279**, 208–211 (1998)
4. Hochbaum, A.I., Chen, R., Delgado, R.D., Liang, W., Garnett, E.C., Najarian, M., Majumdar, A., Yang, P.: Enhanced thermoelectric performance of rough silicon nanowires. Nature **451**, 163–167 (2008)
5. Chan, C.K., Peng, H., Liu, G., McIlwrath, K., Zhang, X.F., Huggins, R.A., Cui, Y.: High-performance lithium battery anodes using silicon nanowires. Nat. Nanotechnol. **3**, 31–35 (2008)
6. Harris, J.T., Hueso, J.L., Korgel, B.A.: Hydrogenated amorphous silicon (a-Si:H) colloids. Chem. Mater. **22**, 6378–6383 (2010)
7. Heitsch, A.T., Fanfair, D.D., Tuan, H.-Y., Korgel, B.A.: Solution–liquid–solid (SLS) growth of silicon nanowires. J. Am. Chem. Soc. **130**, 5436–5437 (2008)
8. Hessel, C.M., Reid, D., Panthani, M.G., Rasch, M.R., Goodfellow, B.W., Wei, J., Fujii, H., Akhavan, V., Korgel, B.A.: Synthesis of ligand-stabilized silicon nanocrystals with size-dependent photoluminescence spanning visible to near-infrared wavelengths. Chem. Mater. **24**, 393–401 (2012)
9. Heath, J.R.: A liquid–solution-phase synthesis of crystalline silicon. Science **258**, 1131–1133 (1992)
10. Zou, J., Baldwin, R.K., Pettigrew, K.A., Kauzlarich, S.M.: Solution synthesis of ultrastable luminescent siloxane-coated silicon nanoparticles. Nano Lett. **4**, 1181–1186 (2004)
11. Baldwin, R.K., Pettigrew, K.A., Ratai, E., Augustine, M.P., Kauzlarich, S.M.: Solution reduction synthesis of surface stabilized silicon nanoparticles. Chem. Commun. **17**, 1822–1823 (2002)
12. Baldwin, R.K., Pettigrew, K.A., Garno, J.C., Power, P.P., Liu, G.Y., Kauzlarich, S.M.: Room temperature solution synthesis of alkyl-capped tetrahedral shaped silicon nanocrystals. J. Am. Chem. Soc. **124**, 1150–1151 (2002)
13. Wilcoxon, J.P., Samara, G.A.: Tailorable, visible light emission from silicon nanocrystals. Appl. Phys. Lett. **74**, 3164–3166 (1999)
14. Tilley, R.D., Warner, J.H., Yamamoto, K., Matsui, I., Fujimori, H.: Micro-emulsion synthesis of monodisperse surface stabilized silicon nanocrystals. Chem. Commun. **14**, 1833–1835 (2005)
15. Fournier, C., Favier, F.: Zn, Ti and Si nanowires by electrodeposition in ionic liquid. Electrochem. Comm. **13**(11), 1252–1255 (2011)
16. Bley, R.A., Kauzlarich, S.M.: Low-temperature solution phase route for the synthesis of silicon nanoclusters. J. Am. Chem. Soc. **118**, 12461–12462 (1996)
17. Mayeri, D., Phillips, B.L., Augustine, M.P., Kauzlarich, S.M.: NMR study of the synthesis of alkyl-terminated silicon nanoparticles from the reaction of SiCl 4 with the Zintl salt, NaSi. Chem. Mat. **13**(3), 765–770 (2001)
18. Lee, S., Cho, W.J., Han, I.K., Choi, W.J., Lee, J.I.: White light emitting silicon nanocrystals as nanophosphor. Phys. Stat. Solid. B **241**, 2767–2770 (2004)
19. Yang, C.S., Bley, R.A., Kauzlarich, S.M., Lee, H.W.H., Delgado, G.R.: Synthesis of alkyl-terminated silicon nanoclusters by a solution route. J. Am. Chem. Soc. **121**(22), 5191–5195 (1999)
20. Pettigrew, K.A., Liu, Q., Power, P.P., Kauzlarich, S.M.: Solution synthesis of alkyl- and alkyl/alkoxy-capped silicon nanoparticles via oxidation of Mg_2Si. Chem. Mat. **15**, 4005–4011 (2003)
21. Dohnalová, K., Poddubny, A.N., Prokofiev, A.A., de Boer, W.D., Umesh, C.P., Paulusse, J.M., Zuilhof, H., Gregorkiewicz, T.: Surface brightens up Si quantum dots: direct bandgap-like size-tunable emission. Light Sci. Appl. **2**, 6378–6383 (2013)
22. McMillan, P.F., Gryko, J., Bull, C., Arledge, R., Kenyon, A.J., Cressey, B.A.: Amorphous and nanocrystalline luminescent Si

and Ge obtained via a solid-state chemical metathesis synthesis route. J. Solid State Chem. **178**, 937–949 (2005)
23. Pelosi, M., Tillard, M., Zitoun, D.: Ge nanoparticles by direct oxidation of Zintl alloys and their electrochemical behavior as anodes of Li-ion batteries. J. Nanopart. Res. **15**, 1872–1883 (2013)
24. Witte, J., von Schnering, H.G., Klemm, W.: Das Verhalten der Alkalimetalle zu Halbmetallen. XI. Die Kristallstruktur von NaSi und NaGe. Z. Anorg. Allg. Chem. **327**, 260–273 (1964)
25. Hohmann, E.: Silicide und Germanide der Alkalimetalle. Z Anorg. Allg. Chem. **257**, 113–126 (1948)
26. Kliche, G., Schwarz, M., von Schnering, H.G.: Raman spectrum of the tetrasilatetrahedrane anion Si_4^{4-}. Angew. Chem. Int. Ed. **26**, 349–351 (1987)
27. Morhange, J.F., Kanellis, G., Balkanski, M.: Raman study of laser annealed silicon. Solid State Commun. **31**(11), 805 (1979)
28. Iqbal, Z., Webb, A.P., Veprek, S.: Polycrystalline silicon films deposited in a glow discharge at temperatures below 250 °C. Appl. Phys. Lett. **36**, 163 (1980)
29. Richter, H., Wang, Z.P., Ley, L.: The one phonon Raman spectrum in microcrystalline silicon. Solid State Commun. **39**, 625–629 (1981)
30. Karmaoui, M., Sá Ferreira, R.A., Mane, A.T., Carlos, L.D., Pinna, N.: Lanthanide-based lamellar nanohybrids: synthesis, structural characterization, and optical properties. Chem. Mater. **18**, 4493–4499 (2006)
31. Ramachandran, G.K., Dong, J.J., Diefenbacher, J., Gryko, J., Marzke, R.F., Sankey, O.F., McMillan, P.F.: Synthesis and X-ray characterization of silicon clathrates. J. Solid State Chem. **145**, 716–730 (1999)
32. Hatchard, T.D., Dahn, J.R.: In situ XRD and electrochemical study of the reaction of lithium with amorphous silicon. J. Electrochem. Soc. **151**, A838–A842 (2004)
33. Jung, H., Park, M., Yoon, Y.-G., Kim, G.-B., Joo, S.-K.: Amorphous silicon anode for lithium-ion rechargeable batteries. J. Power Sources **115**, 346–351 (2003)
34. Kasavajjula, U., Wang, C., Appleby, A.: Nano- and bulk-silicon-based insertion anodes for lithium-ion secondary cells. J. Power Sources **163**, 1003–1039 (2007)
35. Teki, R., Datta, M.K., Krishnan, R., Parker, T.C., Lu, T.-M., Kumta, P.N., Koratkar, N.: Nanostructured silicon anodes for lithium ion rechargeable batteries. Small **5**, 2236–2242 (2009)
36. Graetz, J., Ahn, C.C., Yazami, R., Fultz, B.: Highly reversible lithium storage in nanostructured silicon. Electrochem. Solid-State Lett. **6**, A194–A197 (2003)
37. Wu, H., Chan, G., Choi, J.W., Ryu, I., Yao, Y., McDowell, M.T., Lee, S.W., Jackson, A., Yang, Y., Hu, L., Cui, Y.: Stable cycling of double-walled silicon nanotube battery anodes through solid-electrolyte interphase control. Nat. Nanotechnol. **7**, 310–315 (2012)
38. Martin, C., Crosnier, O., Retoux, R., Bélanger, D., Schleich, D.M., Brousse, T.: Chemical coupling of carbon nanotubes and silicon nanoparticles for improved negative electrode performance in lithium-ion batteries. Adv. Funct. Mater. **21**, 3524–3530 (2011)
39. Li, J., Lewis, R.B., Dahn, J.R.: Sodium carboxymethyl cellulose: a potential binder for si negative electrodes for Li-Ion batteries. Electrochem. Solid-State Lett. **10**, A17–A21 (2007)
40. Lestriez, B., Bahri, S., Sandu, I., Roue, L., Guyomard, D.: On the binding mechanism of CMC in Si negative electrodes for Li-ion batteries. Electrochem. Comm. **9**(12), 2801–2806 (2007)
41. Bridel, J.-S., Azais, T., Morcrette, M., Tarascon, J.-M., Larcher, D.: Key parameters governing the reversibility of Si/Carbon/CMC electrodes for Li-ion batteries. Chem. Mater. **22**(3), 1229–1241 (2010)
42. Guo, J., Wang, C.: A polymer scaffold binder structure for high capacity silicon anode of lithium-ion battery. Chem. Comm. **46**, 1428–1430 (2010)
43. Oumellal, Y., Delpuech, N., Mazouzi, D., Dupré, N., Gaubicher, J., Moreau, P., Soudan, P., Lestriez, B., Guyomard, D.: The failure mechanism of nano-sized Si-based negative electrodes for lithium ion batteries. J. Mater. Chem. **21**(17), 6201–6208 (2011)